Available online at www.sciencedirect.com
SCIENCE DIRECT®
International Journal of Machine Tools & Manufacture 44 (2004) 915–925
INTERNATIONAL JOURNAL OF MACHINE TOOLS & MANUFACTURE DESIGN, RESEARCH AND APPLICATION
www.elsevier.com/locate/ijmactool

Chip formation, cutting forces, and tool wear in turning of Zr-based bulk metallic glass

Mustafa Bakkal [a], Albert J. Shih [b,*], Ronald O. Scattergood [c]

[a] Department of Mechanical and Aerospace Engineering, North Carolina State University, Raleigh, NC 27695, USA
[b] Department of Mechanical Engineering, University of Michigan, Ann Arbor, MI 48109 2136, USA
[c] Department of Materials Science and Engineering, North Carolina State University, Raleigh, NC 27695, USA

Received 23 December 2003; accepted 2 February 2004

Abstract

The chip light emission and morphology, cutting forces, surface roughness, and tool wear in turning of Zr-based bulk metallic glass (BMG) material are investigated. Machining results are compared with those of aluminum 6061-T6 and AISI 304 stainless steel under the same cutting conditions. This study demonstrates that the high cutting speeds and tools with low thermal conductivity and rake angle activate the light emission and chip oxidation in BMG machining. For the BMG chip without light emission, serrated chip formation with adiabatic shear band and void formation is observed. The cutting force analysis further correlates the chip oxidation and specific cutting energy and shows the significant reduction of cutting forces for machining BMG at high cutting speeds. The machined surface of BMG has better surface roughness than that of the other two work materials. Some tool wear features, including the welding of chip to the tool tip and chipping of the polycrystalline cubic boron nitride (PCBN) tool edge, are reported for turning of BMG. This study concludes that BMG can be machined with good surface roughness using conventional cutting tools.

Keywords: Bulk metallic glass; Machining; Cutting forces; Surface roughness; Tool wear

1. Introduction

Bulk metallic glass (BMG) is a new class of engineering material that offers unique mechanical, thermal, magnetic, tribological, and corrosion properties over traditional metals. For example, the Zr-based BMG, the work material used in this study, has high ultimate tensile strength (1900 MPa) [1], high fracture toughness (53 MPa $m^{1/2}$) [2], relatively low density (5900 kg/m^3) [3], high elastic strain limit (2%) [1], and low thermal conductivity (4 W/m-K) [3]. Due to these unique properties, BMG has been investigated for many potential applications.

Machining is a process to fabricate precision BMG components with high dimensional accuracy, complicated shape, and low surface roughness. Due to the low thermal conductivity of BMG, turning experiment shows serrated chip formation, even at low cutting speeds [4]. At high cutting speeds, the BMG chip oxidizes and emits very bright light. The BMG chip remains hot and glowing like a light string for an extended period of time after leaving the tool–workpiece contact region [4,5]. The infrared spectrometer was applied to analyze the thermal radiation spectrum and chip flash temperature. Results showed that the flash temperature of BMG chip with light emission is high, in the 2400–2700 K range. The exothermic oxidation of BMG occurred during the chip formation with light emission [4].

The goal of this research is to study the process conditions that trigger the light emission and analyze the cutting forces, chip morphology, surface roughness, and tool wear in lathe turning of Zr-based BMG. Four cutting tools with different coatings and substrate materials were investigated for turning the $Zr_{52.5}Ti_{5}Cu_{17.9}Ni_{14.6}Al_{10}$ BMG material [6,7]. Two other work

* Corresponding author. Tel.: +1-734-647-1766; fax: +1-734-936-0363.
E-mail address: shiha@umich.edu (A.J. Shih).

0890-6955/$ - see front matter © 2004 Elsevier Ltd. All rights reserved.
doi:10.1016/j.ijmachtools.2004.02.002

Table 1
Properties of three work materials

Material	Elastic modulus (GPa)	Poisson ratio	Strain hardening exponent	Ultimate tensile stress (MPa)	Percent of elongation to fracture	Thermal conductivity (W/m-K)	Vickers hardness (kg/mm^2)	Fracture toughness (MPa m$^{1/2}$)
$Zr_{41.2}Ti_{13.8}Cu_{12.5}Ni_{10.0}Be_{22.5}$ BMG	96	0.36	~0	1900	2 (all elastic)	4	534	40–55
Aluminum 6061-T6	69	0.33	0.23	310	12	167	218	29
AISI 304 stainless steel	193	0.29	0.60	515	40	16.2	200	75–100

materials, the aluminum 6061-T6 and AISI 304 stainless steel, denoted hereafter as Al6061 and SS304, respectively, were machined under identical cutting conditions. These three work materials have distinctly different mechanical and thermal properties, as summarized in Table 1. Comparison of machining results helps to distinguish unique features in BMG machining.

The experimental setup is first introduced. The chip morphology and cutting conditions that initiate chip light emission are studied. Cutting forces of BMG turning are analyzed. Finally, the machined surfaces and tool wear are presented to extract distinctive characteristics in machining the BMG.

2. Experimental setup and design

2.1. Turning test setup and measurements

Turning experiments were conducted in an EMCO PC Turn 125 computer numerical controlled lathe, as shown in Fig. 1(a). Cutting speeds were set at 0.38, 0.76, and 1.52 m/s on the 6.35 mm diameter BMG rod, which was prepared by arc melting method and casting in a Cu mold. The depth of cut, w, was 0.5 mm. The same feed per revolution, t, at 50 μm was used in all cutting tests. The size and shape of BMG, Al6061, and SS304 workpiece and cutting conditions are the same. All cutting tests were conducted dry without using coolant.

Table 2 summarizes the features of four cutting tools, designated as WC-CVD, WC-PVD, PCBN, and PCD, utilized in this study. All the four tools are indexable inserts with 80° rhombic shape. The WC-CVD and WC-PVD tools have the WC in Co matrix as the substrate material. WC-CVD has three layers of chemical vapor deposition (CVD) coatings: TiC in the inside, Al_2O_3 in the middle, and TiN on the outside. The WC-PVD has one layer of the physical vapor deposition (PVD) TiB_2 coating. The other two tool materials are the polycrystalline cubic boron nitride (PCBN) and polycrystalline diamond (PCD). PCBN tool has the TiAlN PVD coating. The PCD tool has no coating. The tool holder has a positive 5° rake angle. The PCBN and PCD inserts have no chip breaker and the rake angle, α, at the cutting edge is 5°. The WC-CVD and WC-PVD tools have a 1 mm wide groove shape chip breaker. The rake angles at the cutting edge for WC-CVD and WC-PVD tools are 12° and 20°, respectively. The PCD has very high thermal conductivity, 560 W/m-K.

As shown in Fig. 1(a), a piezoelectric force dynamometer (Kiestler 9275B) was applied to measure the cutting force, F_c, and feed force, F_f, in the direction parallel and perpendicular to the relative velocity of the tool and workpiece [8]. On the machined surface, the roughness was measured using a Taylor Hobson Talysurf (Model 120) stylus profilometer. The average arithmetic surface roughness, R_a, was recorded with 0.8 mm cut-off length. The average of six measurements was used to represent the surface roughness for

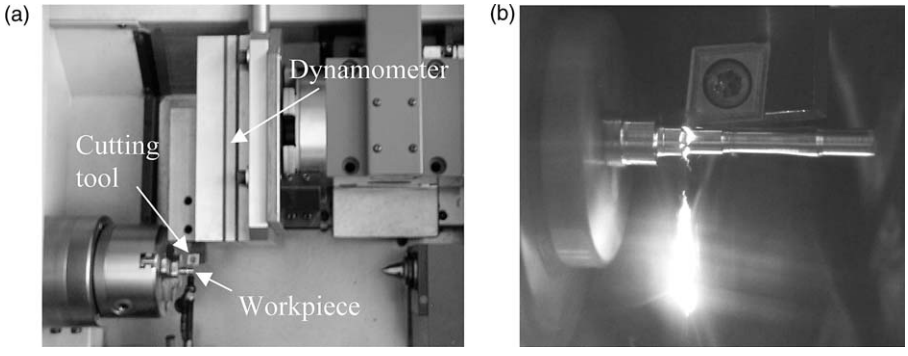

Fig. 1. Lathe turning experiment (a) the setup with dynamometer, cutting tool, and workpiece and (b) light emission from machining of BMG.

Table 2
Four cutting tools used in the turning experiment (tool holder: Seco ISO SCLCL/ANSI 1212F09, insert code: ISO 09T304/ANSI 3251, all inserts have 0.4 mm nose radius)

Tool designation	Material grade	Coating	Chip breaker	Manufacturer	Rake angle (deg)	Substrate thermal conductivity[a] (W/m K)
WC-CVD	CCMT TP15	TiC (base)–Al_2O_3–TiN (top)	7° rake angle	Seco	12	104
WC-PVD	CCGT KC 5410	TiB_2	15° rake angle	Kennametal	20	78
PCD	CCMW KD 100	No coating	No chip breaker	Kennametal	5	560
PCBN	CCGW KB 5615	TiAlN	No chip breaker	Kennametal	5	72

[a] Data provided by manufacturer.

each cutting condition. A Hitachi S-4700 scanning electron microscope (SEM) was used to examine the chip and machined surfaces.

2.2. Experiment design

The three variables in the turning experiment are: (1) four tools (WC-PVD, WC-CVD, PCBN, and PCD), (2) three cutting speeds (0.38, 0.76, and 1.52 m/s), and (3) three work materials (BMG, Al6061, and SS304).

A set of four tests was first conducted using the four tools to cut all three work materials at 1.52 m/s cutting speed. Three additional sets of test were conducted at three cutting speeds (0.38, 0.76, and 1.52 m/s) using the WC-CVD tool for BMG and the WC-PVD tool for Al6061 and SS304. In total, 21 cutting tests were conducted. In each cutting test, the light emission and chip oxidation are observed for BMG, the chips are collected and analyzed using the SEM, the cutting and feed force, chip thickness, and surface roughness are measured, and the tool wear is examined.

3. BMG chip light emission and morphology

The light emission, as shown in Fig. 1(b), is the most distinguishing feature in BMG machining. The work material has significant influence on the chip light emission. No light emission was observed in machining of Al6061 and SS304. For machining BMG, the record of chip light emission and oxidation are summarized in Table 3. The light emission in BMG machining is associated with the chip surface oxidation, which has been investigated by Bakkal et al. [5]. As shown in the mechanical and thermal properties of three work materials in Table 1, the BMG has very low thermal conductivity, which retains the heat in the chip and activates the exothermic oxidation and, consequently, the light emission on the BMG chip surface.

The spectrum of thermal radiation showed the high flash temperature (2400–2700 K) of the BMG chip with light emission during machining [5]. This and the metallurgical analysis of the chip demonstrate that the oxidation of BMG on the chip surface is the source of high flash temperature. Gilbert et al. [9] measured flash temperatures of 3175 K in air and 1400 K in nitrogen on the fracture BMG specimen. The oxidation of fresh material exposed during rupture is the source of light emission.

To further understand the morphology of the chip with and without light emission, the SEM micrographs of BMG chip machined at 1.52 m/s cutting speed using the four tools (WC-PVD, WC-CVD, PCBN, and PCD) are shown in Fig. 2. Each chip sample has three levels of magnification to reveal the details of chip morphology.

From Table 3, three factors that affect the chip light emission in machining BMG are identified.

1. *Cutting speed*: At the lowest cutting speed (0.38 m/s) using the WC-CVD tool, no light emission was observed. At the higher cutting speed at 0.76 and 1.52 m/s, enough energy was delivered to the chip to activate the oxidation and light emission.
2. *Tool rake angle and coating*: The WC-PVD tool has very high rake angle. This generates lower cutting forces, as will be discussed later in Section 4, and less heat in the chip. No chip oxidation and light emission was observed for BMG machined by WC-PVD tool. Also, the TiB_2 coating on WC-PVD tool has high thermal conductivity (130 W/m-K vs. 20–28 and 19–21 W/m-K of Al_2O_3 and TiN,

Table 3
Light emission and chip surface oxidation in BMG machining

Cutting tool	Cutting speed (m/s)	Light emission	Chip surface oxidation
WC-CVD	0.38	No	No
	0.76	Yes	Yes
	1.52[a]	Yes	Yes
WC-PVD	1.52[a]	No	No
PCBN	1.52[a]	Yes	Yes
PCD	1.52[a]	No[b]	No

[a] SEM micrographs of the chip shown in Fig. 2.
[b] Some light emission at the start of cutting.

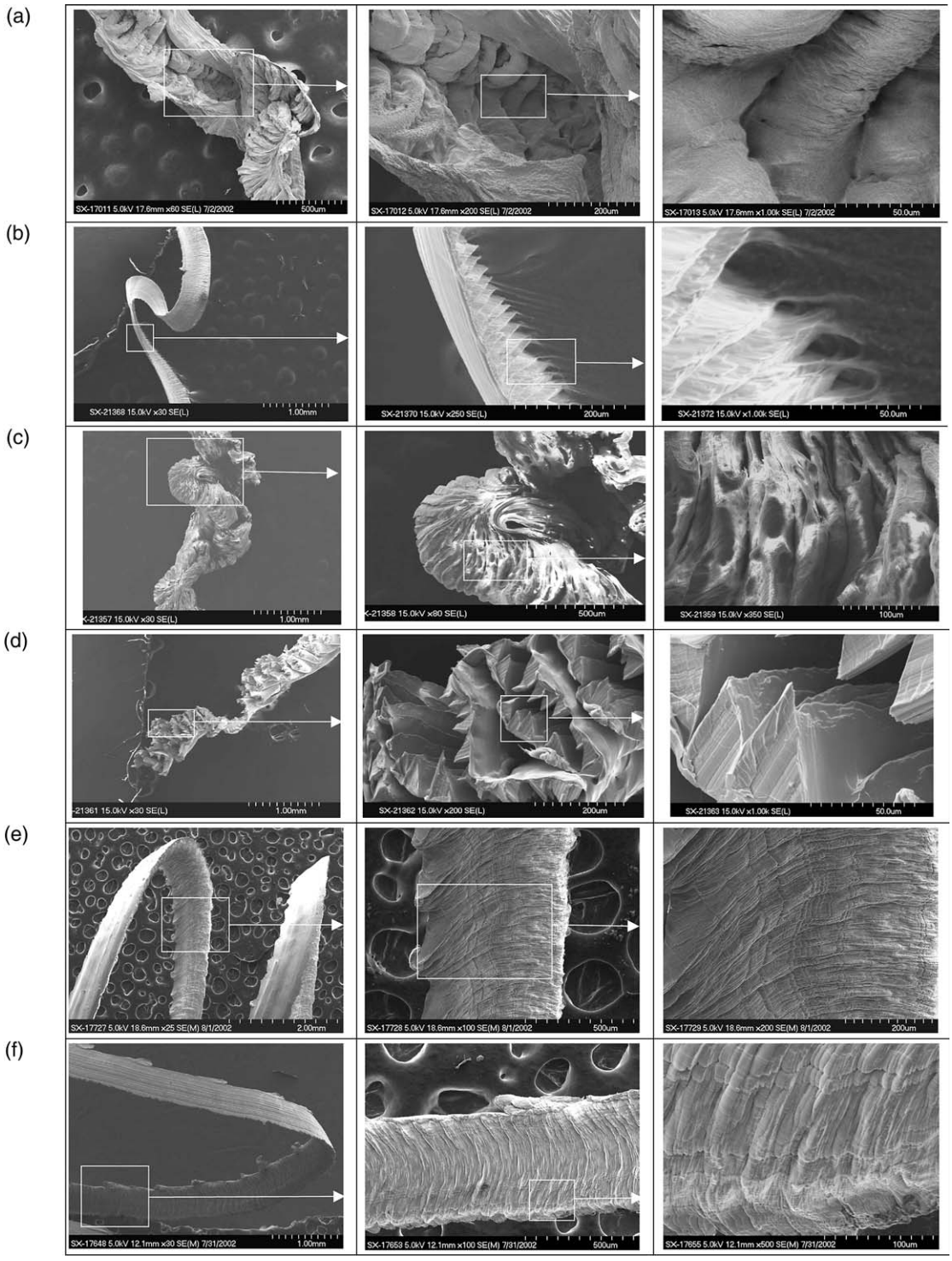

Fig. 2. SEM micrographs of BMG, Al6061, and SS304 chips machined at 1.52 m/s cutting speed; (a) Workpiece: BMG; tool: WC-CVD; with chip light emission; (b) Workpiece: BMG; tool: WC-PVD; no chip light emission; (c) Workpiece: BMG; tool: PCBN; with chip light emission; (d) Workpiece: BMG; tool: PCD; no chip light emission; (e) Workpiece: A16061; tool: WC-CVD; no chip light emission; (f) Workpiece: SS304; tool: WC-CVD; no chip light emission.

respectively) and is resistant to the chip sticking during machining [10,11]. This type of coating is used extensively for machining of Al due to the chemical stability with Al at high temperature. More research

is required to distinct the rake angle and coating effects in BMG machining.

3. *Tool thermal conductivity*: Under identical tool geometry and cutting condition, the PCD tool does not generate the chip light emission as the PCBN tool. The high thermal conductivity of the PCD tool, 560 vs. 72 W/m-K of PCBN tool (see Table 1), is the likely key factor. At the tool–chip interface, more heat is conducted to the tool with higher thermal conductivity. This reduces the chip temperature and retards the BMG chip oxidation and light emission.

Two distinct types of BMG chip morphology can be identify in Fig. 2. For the BMG chips with light emission, such as those machined by WC-CVD and PCBN tools (Fig. 2(a), (c)), rounded edges indicate the partial melting of the work material. For the BMG chips with no light emission, such as those cut by WC-PVD and PCD tools (Fig. 2(b), (d)), serrated chip formation with the sharp edge and shear localization is observed. In comparison, chips generated by Al6061 and SS304 (Fig. 2(e), (f)) under the same cutting speed and feed have the typical curled shape with no serration.

The serrated BMG chip produced during cutting without light emission is likely due to the very low thermal conductivity of the BMG (4 W/m-K). The serrated chip formation is similar to that of Ti and nickel-based alloys, which has the low thermal conductivity at about 7 and 10 W/m-K, respectively. Like the machined chip of Ti and nickel-based alloys, the shear localization (adiabatic shear band) in serrated BMG chip is due to the thermal instability of the low thermal conductivity work material during machining [12–17]. Comparing the serrated BMG chips in Fig. 2(b), (d), the shear lamella in Fig. 2(d) almost came apart and was just held by very thin back of the chip. The cutting tool geometry with and without groove for chip breaking, rake angle, and thermal conductivity of tool materials all contribute to the difference. SS304 has also shear localization due to relatively low thermal conductivity. The BMG chip shows more dramatic shear localization than the SS304 chip.

Chip curl is another feature of the BMG chip. Unlike the Al6061 and SS304 chips (Fig. 2(e), (f)), the BMG chip does not curl consistently. The BMG chip cut by WC-PVD tool shows the random curl of the chip in two directions. The BMG chip cut by PCD tool has the unique feature of tightly folded serrated BMG chip. This chip folding is more obvious in the close-up view.

In Fig. 2(b), the close-up view of the BMG chip machined by WC-PVD showed the void formation. The size of the void is from 10 to 40 μm. Void formation and adiabatic shear band on the fractured surface has been observed on the fractured surface of BMG tensile test samples [18] and BMG chip [4]. Two hypotheses for localized shear band formation in BMG have been proposed [18]. The first hypothesis assumes that the viscosity decreases due to the creation of free volume and void formation within the shear bands. The second hypothesis contributes the shear band formation to the thermal softening and adiabatic heating. The void formation obviously contributes to the BMG chip machined by WC-PVD tool. The average atomic volume inside an active (deforming) shear band is larger than in an undeformed region. This excess free volume results in the rapid viscosity decrease and localization of shear deformation. When the stress is removed, the excess free volume becomes thermodynamically unstable, and there is a large driving force for the nucleation of voids as the shear band relaxes.

For the oxidized BMG chip machined by WC-CVD and PCBN tools (Fig. 2(a), (c)), SEM micrographs in Fig. 2 show that the shear band still exists among the twisted and tangled lamellae surrounded by regions of viscous-like molten and solidified BMG material. The shear localization is likely caused by the second hypothesis, i.e., the thermal softening and adiabatic heating since no void could be seen. The metallurgical analysis of the molten BMG chip has been conducted by Bakkal et al. [4]. An oxide layer is surrounding the chip. Inside the chip, crystallization of the BMG may occur in some fast cooling regions.

4. Cutting forces and discussions

4.1. Analytical analysis of cutting forces and stresses

The measured cutting and feed force data for three work materials are not steady-state during machining. As shown in the sample cutting and feed forces data in Fig. 3, for machining of BMG by the PCD tool at 1.52 m/s cutting speed, the cutting and feed forces exhibit large variation in the first 0.5 s after the initial contact of tool and workpiece. The average of force 1 s after the contact is used to represent the BMG cutting and feed forces. For machining of Al6061 and SS304, the gradual increase of forces due to strain hardening is observed. An example is the forces generated by PCBN machining of SS304 in Fig. 3. A range of cutting and feed forces is reported for cutting of Al6061 and SS304. Results of cutting and feed forces as well as the specific cutting energy are summarized in Table 4.

The measured cutting force (F_c) and feed force (F_f) are transformed to the normal force and friction force on the tool rake face, denoted as F and N, respectively.

$$F = F_c \sin\alpha + F_f \cos\alpha \quad (1)$$

$$N = F_c \cos\alpha + F_f \sin\alpha \quad (2)$$

The coefficient of friction on the rake face $\mu = F/N$.

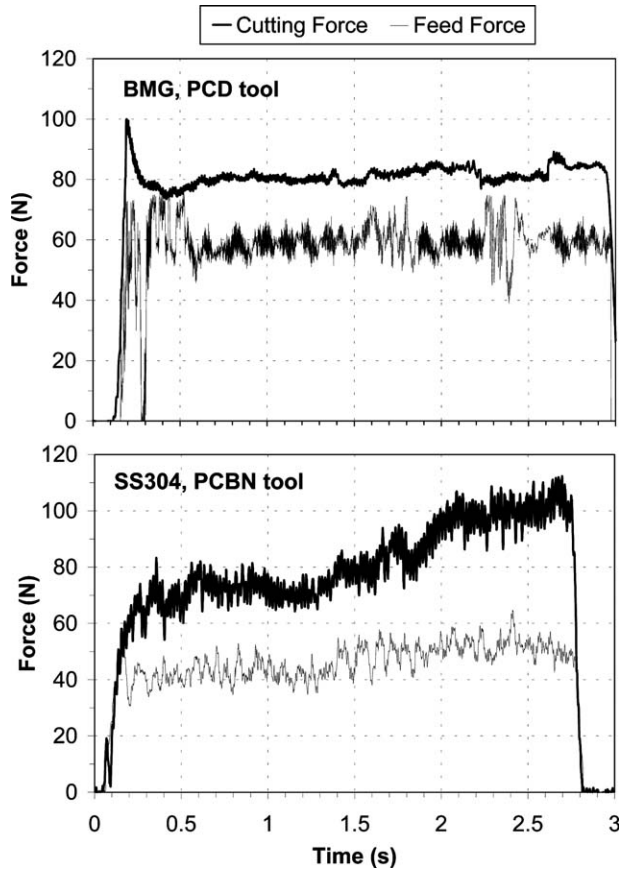

Fig. 3. Sample cutting and feed forces of BMG machined by the PCD tool and SS304 machined by PCBN tool at 1.52 m/s cutting speed.

The specific cutting energy, u_s, which represents the energy required to remove a unit volume of work material, is calculated from the cutting force (F_c), feed (t), and depth of cut (w).

$$u_s = \frac{F_c}{wt} \tag{3}$$

4.2. Cutting force results and discussions

4.2.1. Cutting and feed forces

Table 4 summarizes results of the cutting and feed forces and specific cutting energy. For all three work materials, the high rake angle of WC-PVD tool (20°) generates noticeably lower cutting and feed forces and specific cutting energy than the other three tools. For machining BMG, lower cutting forces represent that less energy enters into the same volume of work material. As shown in Table 3 and Fig. 2(b), the BMG chip machined by the WC-PVD tool does not have the oxidation and associated light emission. On the contrary, the BMG machined by WC-CVD tool has the highest level of specific cutting energy and the most significant melting and burning of chip (Fig. 2(a)). Comparing the PCBN and PCD tools with the same geometry for BMG machining, the PCD tool generates slightly higher cutting force and specific cutting energy. The TiAlN coating on the PCBN tool is the likely cause for lower cutting forces. The high thermal conductivity of the PCD helps to absorb part of the energy to avoid triggering the chip oxidation.

Table 4
Cutting and feed forces and specific cutting energy

Tool materials[a]		WC-CVD	WC-PVD	PCBN	PCD
BMG	F_c (N)	110	36	70	81
	F_f (N)	100	23	50	59
	u_s (MJ/m^3)	4300	1400	2700	3100
Al6061	F_c (N)	50–65	37–40	40–80	28–30
	F_f (N)	30–50	22–28	25–40	14–16
	u_s (MJ/m^3)	1900–2500	1400–1500	1600–3100	1100–1200
SS304	F_c (N)	55–75	68–71	70–90	60–80
	F_f (N)	35–50	34–40	40–50	40–65
	u_s (MJ/m^3)	2200–2900	2600–2800	2700–3500	2300–3100
Cutting speed (m/s)		0.38	0.76	1.52	
BMG (WC-CVD)[b]	F_c (N)	194	180	110	
	F_f (N)	135	130	100	
	u_s (MJ/m^3)	7500	7000	4300	
Al6061 (WC-PVD)[b]	F_c (N)	28–34	38–40	37–40	
	F_f (N)	16–22	24–27	22–28	
	u_s (MJ/m^3)	1100–1300	1500–1600	1400–1500	
SS304 (WC-PVD)[b]	F_c (N)	72–74	65–68	68–71	
	F_f (N)	48–51	36–44	34–40	
	u_s (MJ/m^3)	2800–2900	2500–2600	2600–2800	

[a] At 1.52 m/s cutting speed.
[b] In parentheses: tool material used.

The PCD tool was known for machining of aluminum [19]. Therefore, comparing the cutting forces generated by PCD and PCBN tools, which have identical tool geometry, the PCD exhibits much lower forces for Al6061.

Across three work materials at 1.52 m/s cutting speed, the cutting and feed forces for BMG are generally higher than Al6061 but lower than SS304. This indicates that, from the cutting force point of view, the BMG can be machined like other metallic materials.

The second part of Table 4 shows the effect of cutting speed. For BMG, the cutting and feed forces and specific cutting energy decreases at higher cutting speeds. This is due to the thermal softening of the low thermal conductivity work materials at high cutting speeds [8]. Kato et al. [20] and Kawamura et al. [21] have observed the drastic reduction of BMG viscosity at high strain rate and temperature. The thermal conductivity does not severely affect cutting forces on SS304 cutting as observed on BMG cutting. Flow stress changing is more effective in SS304 cutting than BMG due to the strain hardening. Opposite trend of higher cutting forces at lower cutting speed is observed for Al6061. The balance of strain rate hardening and thermal softening causes such different trends. For the low thermal conductivity BMG and SS304, the heat generated during machining cannot be transferred quickly to the tool and surroundings. It causes the localized high temperatures in the chip deformation zones and, therefore, creates the thermal softening and instability.

4.2.2. Specific cutting energy

The specific energy required to melt a unit volume of BMG, Al6061, and SS304 from 30 °C to the melting temperature of each work material is estimated as 4060, 2510, and 5900 MJ/m^3, respectively [22,23]. For machining using the sharp WC-PVD tool, as shown in Table 4, the specific cutting energy is about half of the specific melting energy. Machining using the WC-CVD tool generates the highest specific cutting energy, about the same as the specific melting energy.

The cutting speed effect is different for three work materials. For BMG, due to the thermal softening, machining at high speed significantly reduces the specific cutting energy. A different trend is observed on Al6061, a material with much higher thermal conductivity and less thermal softening effect. For SS304, the effect of cutting speed on specific cutting energy is not obvious due to the balance of thermal softening and strain rate hardening effect.

The significant reduction in specific cutting energy for BMG from 7500 and 7000 MJ/m^3 at two lower cutting speeds to 4300 MJ/m^3 at the highest cutting speed can correlate to the chip formation. At low cutting speeds, the BMG chip morphology is serrated and has sharp edges [5]. While at high cutting speed, as shown in Fig. 2(a), the chip has significant local melting, which, in turn, softens the work material and reduces the specific cutting energy.

4.2.3. Normal and friction force on the rake face and coefficient of friction

Table 5 shows the normal and friction forces on the tool rake face, calculated using Eqs. (1) and (2). The high rake angle WC-PVD tool generates the lowest normal and shear force on the rake face but does not lower coefficient of friction. The effect of high rake angle on high coefficient of friction, above 1.0, is consistent with the observation and discussion by Bailey [24].

The two hard tools, PCD and PCBN, consistently show the benefit of lower coefficient of friction for machining of three work materials.

The effect of cutting speed on coefficient of friction at tool rake surface is mixed, which has also been observed by Bailey [24]. For BMG and Al6061, high cutting speed increases the coefficient of friction. The opposite trend occurs for SS304. The cutting speed has more significant effect on the reduction of normal force for BMG than SS304, i.e., at higher cutting speeds, N is reduced for BMG but remains about the same for SS304. This, coupled with fact that the friction force, F, is lowered for both BMG and SS304, generates the mixed effect of cutting speed on coefficient of friction for BMG and SS304.

4.2.4. Shear plane angle and average normal and shear stress on the shear plane

Using the measured chip thickness, an imaginary shear plane can be created and the shear plane angle, ϕ, can be estimated. For Al6061 and SS304, the shear angle is between 15° and 20°, which matches the previous findings [19,25]. For BMG under the same cutting condition, the chip thickness is generally thinner and shear angle is expected to be larger. The accurate measurement of BMG chip thickness is difficult due to its brittleness and serrated shape.

The average cutting and feed forces can be transformed to force components normal and perpendicular to the shear plane. These two force components are divided by the area of the shear plane to calculate the average normal and shear stress on the shear plane. For Al6061 and SS304, the calculated normal and shear stresses on the shear plane are ranging from 0.2 to 0.7 and 0.4 to 0.9 GPa, respectively. The results match the data reported by Childs et al. [26].

5. Surface roughness analysis

The effect of cutting speed and tool material and coating on surface finish is investigated. All surfaces

Table 5
Normal and friction force and coefficient of friction on rake plane

Tool materials[a]		WC-CVD	WC-PVD	PCBN	PCD
BMG	Normal force, N (N)	87	26	65	76
	Friction force, F (N)	121	34	56	66
	Coefficient of friction, μ	1.4	1.3	0.9	0.9
Al6061	Normal force, N (N)	43–53	27–28	38–76	27–28
	Friction force, F (N)	39–62	33–40	28–47	16–19
	Coefficient of friction, μ	0.9–1.1	1.2–1.4	0.6–0.7	0.6–0.7
SS304	Normal force, N (N)	47–63	52–53	66–85	56–74
	Friction force, F (N)	46–65	55–62	46–58	45–72
	Coefficient of friction, μ	0.9–1.0	1.1–1.2	0.7–0.8	0.8–1.0
Cutting speed (m/s)		0.38	0.76	1.52	
BMG (WC-CVD)[b]	Normal force, N (N)	162	149	87	
	Friction force, F (N)	172	165	121	
	Coefficient of friction, μ	1.1	1.1	1.4	
Al6061 (WC-PVD)[b]	Normal force, N (N)	21–24	28–29	27–28	
	Friction force, F (N)	25–32	36–39	33–40	
	Coefficient of friction, μ	1.2–1.3	1.3–1.4	1.2–1.4	
SS304 (WC-PVD)[b]	Normal force, N (N)	51–52	49–50	52–53	
	Friction force, F (N)	70–73	56–65	55–62	
	Coefficient of friction, μ	1.3–1.4	1.2–1.3	1.1–1.2	

[a] At 1.52 m/s cutting speed.
[b] In parentheses: tool material used.

were machined under the same feed (50 μm) and tool nose radius (0.4 mm). The theoretically arithmetic average surface roughness R_a of a surface consisting of circular arcs generated based on the tool tip radius and feed is 0.2 μm [27]. This ideal value is lower than the actual measured and averaged R_a of machined surfaces, as summarized in Table 6.

For the BMG surfaces, higher R_a can be observed on the two tools (WC-PVD and PCD) that generate serrated BMG chip. It is possible that the periodically shear band formation generates dynamic motion at the tool tip and deteriorates the surface roughness. The WC-CVD tool, which creates the most severe burning of the chip (shown in Fig. 2(a)), has the best R_a of 0.47 μm. The cutting speed also affects BMG surface roughness. For the BMG machined by WC-CVD tool, the high cutting speed generates a rougher surface. Among all experiments, BMG machined by WC-CVD tool at 0.38 m/s has the lowest R_a of 0.35 μm. It is still higher than the ideal value of 0.2 μm R_a. The good surface roughness on machined BMG surface indicates that

Table 6
Average arithmetic surface roughness

Tool materials[a]		WC-CVD	WC-PVD	PCBN	PCD
BMG	R_a (μm)	0.47	0.84	0.53	0.62
	R_a range (μm)	0.42–0.49	0.82–0.85	0.51–0.56	0.54–0.68
Al6061	R_a (μm)	1.17	0.85	1.06	1.07
	R_a range (μm)	1.05–1.23	0.82–0.86	1.05–1.13	0.90–1.14
SS304	R_a (μm)	2.71	2.53	0.58	1.50
	R_a range (μm)	2.60–2.95	2.24–2.58	0.53–0.62	1.49–1.51
Cutting speed (m/s)		0.38	0.76	1.52	
BMG (WC-CVD)[b]	R_a (μm)	0.35	0.42	0.47	
	R_a range (μm)	0.32–0.39	0.41–0.44	0.42–0.49	
Al6061 (WC-PVD)[b]	R_a (μm)	0.77	0.82	0.85	
	R_a range (μm)	0.75–0.78	0.78–0.83	0.82–0.86	
SS304 (WC-PVD)[b]	R_a (μm)	1.68	3.22	2.53	
	R_a range (μm)	1.46–1.74	2.77–3.61	2.24–2.58	

[a] At 1.52 m/s cutting speed.
[b] In parentheses: tool material used.

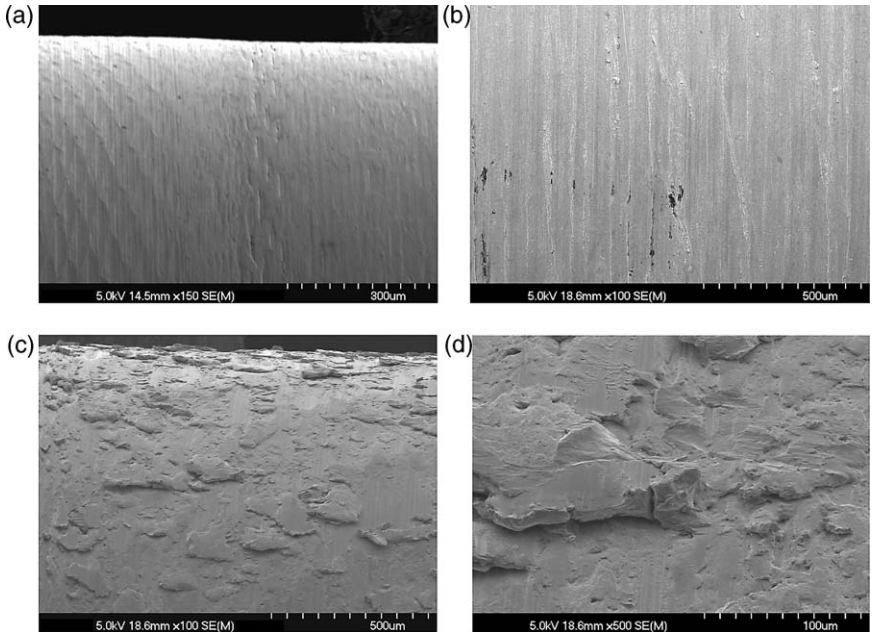

Fig. 4. The WC-CVD tool machined surfaces at 0.76 m/s cutting speed. (a) BMG, 0.42 μm R_a; (b) A16061, 0.82 μm R_a; (c) SS304, 3.22 μm R_a; (d) SS304 (close-up view).

machining can be used for BMG material to generate very smooth surface for various potential applications.

Among the three work materials machined under the same setup, the surface roughness of SS304 is generally higher. As an austenitic stainless steel, as shown in Table 1, SS304 has the highest strain hardening rate (0.6), fracture toughness (100 MPa $m^{1/2}$ K_{IC}), and ductility (40% elongation to fracture) among the three work materials [28]. The only exception on the surface roughness of SS304 is the use of PCBN tool with TiAlN coating. The TiAlN tool coating, which has been demonstrated beneficial by Castanho and Vieira [29] for machining of stainless steel, generates low surface roughness (0.58 μm R_a) for machining SS304.

The SEM micrographs of the surface of three work materials machined by WC-CVD at 0.76 m/s are shown in Fig. 4. Regular lathe turned surfaces with groove marks are observed for the BMG and Al6061 in Fig. 4(a), (b), respectively. The very rough surface, 3.22 μm R_a, on the SS304 surface is obviously caused by nodules on the machined surface, as shown in Fig. 4(c). A close-up view of a nodule, as shown in Fig. 4(d), illustrates that it is created by the residual chip sticking from the surface due to the high ductility of SS304.

6. Tool wear

Due to the limited availability of BMG material, an extensive study of tool wear for machining of BMG was not possible in this study. Only a few observations on the tool wear and breakage during the turning tests are summarized. First, the BMG chip can weld to the tool at the end of a cutting operation. Fig. 5 shows a WC-CVD tool with a string of BMG chip welded to the tool tip. Significant melting, as shown in Fig. 2(a), occurs on the BMG chip machined by WC-CVD. This promotes the welding of the chip to the tool tip, which likely occurs at the end of the cutting process.

The SEM micrograph of PCBN tool used after machining BMG is shown in Fig. 6. The chipping at cutting edge is observed not only around the tool nose radius region, where most of the cutting action occurs, but also along the cutting edge adjacent to the tool tip. This area does not have the physical contact with the workpiece. The chipping is likely caused by the impact of BMG chip with the tool edge during machining.

Fig. 5. BMG chip welded on the WC-CVD tool.

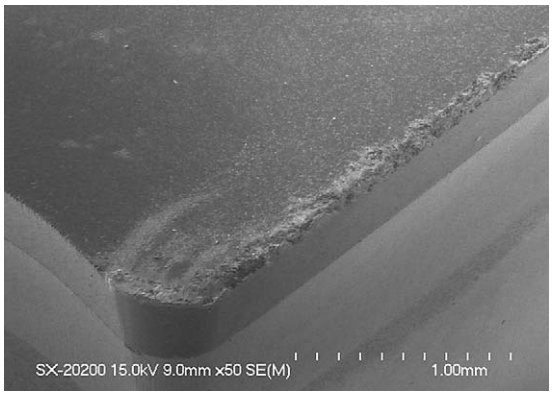

Fig. 6. PCBN tool after machining the BMG.

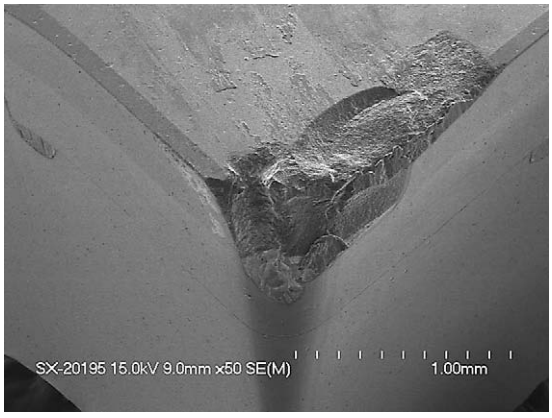

Fig. 7. PCD tool after machining, in sequence, BMG, Al6061 and SS304.

The PCD tool is used to machine BMG first, then Al6061, and finally SS304. After machining BMG and Al6061, minor edge chipping, similar to that showed in PCBN tool in Fig. 6, was observed. However, during machining SS304, the catastrophic breakage of the PCD tool tip occurred, as shown in Fig. 7. This demonstrated that diamond is not suitable to machine ferrous material due to the graphitization of diamond over 730 °C in contact with iron [8,25].

7. Concluding remarks

In this study, the lathe turning of BMG using four tools at three cutting speeds was investigated. The effect of cutting speed, tool rake angle and coating, and tool thermal conductivity on the BMG chip oxidation and light emission was analyzed. Chip morphology showed that the light emission is correlated to the melting of BMG chip. For the BMG chip without light emission, the serrated chip with adiabatic shear band and void formation was observed. Cutting forces and specific cutting energy of BMG is compared with those of Al6061 and SS304. High cutting speed significantly reduced the forces for BMG machining due to thermal softening.

Roughness of machined BMG surfaces is generally better than the other two work materials. This indicated the potential to use BMG for single point diamond turning of very precise surface for optical and photonic applications. Tool wear, like in machining of titanium and nickel-based alloys, is expected to be a problem for machining of BMG. Limited machining of BMG already showed the chipping on the tool cutting edge.

Preliminary study has been conducted for BMG drilling, which is another important machining process for fabrication of BMG into precise, useful components. All test results indicate that BMG can be manufactured using the machining processes to generate high dimensional accuracy with good surface roughness.

Acknowledgements

The tooling and technical support from Parag Hegde of Kennametal are greatly appreciated. A portion of this research was sponsored by the Heavy Vehicle Propulsion Systems Materials Program, Office of Transportation Technologies, US Department of Energy and by the Assistant Secretary for Energy Efficiency and Renewable Energy, Office of Transportation Technologies, as part of the High Temperature Materials Laboratory User Program, Oak Ridge National Laboratory, managed by UT-Battelle, LLC for the US Department of Energy under contract number DE-AC05-00OR22725.

References

[1] H.A. Bruck, T. Christman, A.J. Rosakis, W.L. Johnson, Quasi-static constitutive behavior of Zr41.25Ti13.75Ni10Cu12.5Be22.5 bulk amorphous alloys, Scripta Materialia 30 (1994) 429–434.
[2] C.J. Gilbert, R.O. Ritchie, W.L. Johnson, Fracture toughness and fatigue-crack propagation in a Zr–Ti–Ni–Cu–Be bulk metallic glass, Applied Physics Letters 71(4) (1997) 476–478.
[3] C.C. Aydiner, E. Ustundag, M.B. Prime, A. Peker, Modelling and measurement of residual stresses in a bulk metallic glass plate, Journal of Non-Crystalline Solids 316 (2003) 82–95.
[4] M. Bakkal, C.T. Liu, T.R. Watkins, R.O. Scattergood, A.J. Shih, Oxidation and crystallization of Zr-based bulk metallic glass due to machining, Intermetallics 12 (2004) 195–204.
[5] M. Bakkal, A.J. Shih, R.O. Scattergood, C.T. Liu, Machining of a Zr–Ti–Al–Cu–Ni metallic glass, Scripta Materialia 50 (2004) 583–588.
[6] X.L. Lin, W.L. Johnson, W.K. Rhim, Effect of oxygen impurity on crystallization of an undercooled bulk glass forming Zr–Ti–Cu–Ni–Al alloy, Materials Transactions, JIM 38 (1997) 478–482.

[7] C.T. Liu, L. Heatherly, D.S. Easton, C.A. Carmichael, J.H. Chen, C.H. Chen, J.L. Wright, M.H. Yoo, J.A. Horton, A. Inoue, Test environments and mechanical properties of Zr-base bulk amorphous alloys, Metallurgical and Materials Transactions 29(A) (1998) 1811–1820.
[8] E.M. Trent, P.K. Write, Metal Cutting, Butterworth-Heineman, Boston, 2000.
[9] G.J. Gilbert, J.W. Ager, V. Schroeder, R.O. Ritchie, J.P. Lloyd, J.R. Graham, Light emission during fracture of a Zr–Ti–Ni–Cu–Be bulk metallic glass, Applied Physics Letters 74 (1999) 3809–3811.
[10] M. Berger, M. Larsson, S. Hogmark, Evaluation of magnetron-sputtered TiB2 intended for tribological applications, Surface and Coatings Technology 124 (2000) 253–261.
[11] R.K. Williams, R.S. Graves, F.J. Weaver, Transport properties of high purity polycrystalline titanium diboride, Journal of Applied Physics 59(5) (1986) 1552–1556.
[12] R. Komanduri, R.H. Brown, On the mechanics of chip segmentation in machining, Journal of Engineering for Industry 103 (1981) 33–51.
[13] J. Sheikh-Ahmad, J.A. Bailey, Flow instability in the orthogonal machining of CP titanium, Journal of Manufacturing Science and Engineering 119 (1997) 307–313.
[14] L.N. Lopez de lacalle, J. Perez, J.I. Llorente, J.A. Sanchez, Advanced cutting conditions for the milling of aeronautical alloys, Journal of Materials Processing Technology 100 (2000) 1–11.
[15] R. Shivpuri, J. Hua, P. Mittal, A.K. Srivastava, G.D. Lahoti, Microstructure–mechanics interactions in modeling chip segmentation during titanium machining, Annals of CIRP 51(1) (2002) 71–74.
[16] I.A. Choudhury, M.A. El-Baradi, Machinability of nickel-base super alloys: a review, Journal of Materials Processing Technology 77 (1998) 278–284.
[17] R. Komanduri, T.A. Schroeder, On shear instability in machining nickel-based superalloy, Journal of Engineering of Industry 108 (1986) 93–100.
[18] W.J. Wright, R. Saha, W.D. Nix, Deformation mechanisms of the Zr40Ti14Ni10Cu12Be24 bulk metallic glass, Materials Transactions 42 (2001) 642–649.
[19] C.H. Shen, The importance of diamond coated tools for agile manufacturing and dry machining, Surface and Coatings Technology 86–87 (1996) 672–677.
[20] H. Kato, Y. Kawamura, A. Inoue, H.S. Chen, Newtonian to non-Newtonian master flow curves of a bulk glass alloy $Pd_{40}Ni_{10}Cu_{30}P_{20}$, Applied Physics Letters 73(25) (1998) 3665–3667.
[21] Y. Kawamura, T. Shibata, A. Inoue, T. Masumoto, Deformation behavior of Zr65Al10Ni10Cu15 glassy alloy with wide supercooled liquid region, Applied Physics Letters 69(9) (1996) 1208–1210.
[22] R. Busch, Y.J. Kim, W.L. Johnson, Thermodynamics and kinetics of the undercooled liquid and the glass transition of the Zr41.2Ti13.8Cu12.5Ni10.0Be22.5 alloy, Journal of Applied Physics 77(8) (1995) 4039–4043.
[23] F. Cverna, Thermal Properties of Metals, ASM International Materials Park, Ohio, 2002.
[24] J.A. Bailey, Friction in metal machining: mechanical aspects, Wear 31 (1975) 243–275.
[25] M.C. Shaw, Metal cutting principles, Oxford, 1984.
[26] T.H.C. Childs, K. Maekawa, T. Obikawa, Y. Yamane, Metal Machining, Theory and Application, Arnold, London, 2000.
[27] J. Qu, A.J. Shih, Analytical surface roughness parameters of a theoretical profile consisting of elliptical arcs, Machining Science and Technology 7(2) (2003) 281–294.
[28] J.R. Davis, ASM Specialty Handbook, Stainless Steels, ASM International, Ohio, 1994.
[29] J.M. Castanho, M.T. Vieira, Improving the cutting performance of TiAlN coatings using submicron metal interlayers, Key Engineering Materials 230–232 (2002) 635–639.